Wavelet-Based Higher Order Correlative Stacking for Seismic Data Denoising in the Curvelet Domain

Jing-He Li, Yu-Jie Zhang, Rui Qi, and Qing Huo Liu, *Fellow, IEEE*

***Abstract*—To whiten random noise and identify coherent noise while preserving the features of seismic events, a hybrid denoising scheme of wavelet-based higher order correlative stacking (HOCS) in the curvelet domain is proposed. The proposed algorithm uses HOCS to isolate the coefficients of seismic events in the curvelet domain. It then removes the noises and recovers signals recorded in noisy environment, without the need to choose an arbitrary threshold; the HOCS method selects a threshold automatically in the curvelet domain. Therefore, with the HOCS, it is possible to capture the features of useful signals with good correlations at all scales and all angles, then to remove the features of coherent noise with disordered correlations. Using interpretive seismic records of karst cavities and hidden sinkhole detections after artificial backfill, we show that the proposed scheme improves noisy seismic data significantly with respect to both signal-to-noise ratio and fidelity. To demonstrate the advantages of this hybrid denoising scheme, a comparison of the performances between different individual denoising methods is investigated for complex seismic records contaminated with different types of noise. Numerical case studies and three field data examples validate the effectiveness of the hybrid denoising scheme proposed in this paper.**

***Index Terms*—Filter noise, geophysical signal processing , higher order statistics, seismic signal processing.**

I. Introduction

DENOISING is a common aspect of data processing in fields such as geophysical exploration, biomedical detection, and image denoising [1]–[5]. In seismic exploration, wave fronts are intermixed with random and coherent noises (adaptively scaled Gaussian noise) introduced by the acquisition system and other sources of measurement uncertainty. Thus, seismic denoising aims at recovering damaged segments of continuous seismic data, although this remains a basic and challenging aspect of seismic data processing [6]–[11].

Numerous algorithms have been developed to make this problem more tractable. One class of univariate denoising methods has been developed, such as the K-L (Karhunen–Lòeve) transforms, F-X (frequency-space) deconvolution, and τ-P (linear Radon transform) transform [1]. Such traditional denoising methods take advantage of simple orthogonal transforms, but fail to deal with complicated events with curved or conflicting dips [1], [12]. Wavelet-based algorithms comprise another class of denoising algorithm that has been used in a wide range of seismic applications in recent decades [2], [13]–[16]. However, a one-dimensional (1-D) wavelet is only well-suited for singularity detection using individual trace processing [1], [17]. A two-dimensional (2-D) wavelet transform can be expressed in terms of a tensor integral of discrete 1-D wavelets [18], [19]; thus, this kind of 2-D representation cannot be utilized to reconstruct line-shaped edge features [20], [21].

Investigating seismic records with correlative statistics, based on the theory of second-order stacking, is another method for the suppression of incoherent noise [22]. Higher order correlative stacking (HOCS) has been applied to coherent noise in the wavelet domain to denoise seismic [23], [24] and electromagnetic data [25]. However, for damaged or missing seismic records, it is difficult to estimate the continuous correlation by using the HOCS method. To the best of our knowledge, such a denoising scheme, incorporating the HOCS method for the reconstruction of damaged seismic data, has not been previously reported, and this is one contribution of the present work.

For resolving complicated problems, such as the uncontinuous or damaged events in noisy environments, seismic denoising involves both the retention of useful information and multiscale and multidirectional implementation [26]. Thus, the curvelet transform has been used extensively in seismic data denoising problems in the past decade [27]–[29]. Compared with the wavelet transform, the curvelet transform not only relates to position and frequency, but is controlled by the translation angle. With such a unique advantage, curvelets have been used for ground roll removal [30]–[32], coherent noise removal [33], [34], and separation of overlapping events [35], [36]. However, an appropriate choice of a hard threshold is a basic requirement, and this presents a challenging task in curvelet denoising. Curvelets are also not suggested for denoising point-like features due to their intrinsic properties [1].

To overcome these shortcomings, many methods have been proposed for seismic denoising, including multichannel singular spectrum analysis [37], [38], the modified F-K transform [39], and other methods [40]–[42]. One such approach is denoising that works in multiple domains based on different fields, which aims at obtaining better results [43], [44]. Among the

Manuscript received December 6, 2016; revised January 8, 2017 and February 5, 2017; accepted March 17, 2017. Date of publication April 11, 2017; date of current version August 9, 2017. This work was supported in part by the Natural Science Fund of Guangxi under Grant 2016GXNSFBA380195, in part by the Nature Science Foundation under Grant 41604097, and in part by the China Postdoctoral Science Foundation under Grant 2016M592611. *(Corresponding author: Jinghe Li.)*

J.-H. Li is with the College of Earth Science, Guilin University of Technology, Guilin 541004, China (e-mail: jinghelee7513@gmail.com).

Y.-J. Zhang is with the School of Mathematics and Physics, China University of Geosciences, Wuhan 430074, China (e-mail: zhangyujie@cug.edu.cn).

R. Qi is with the Institute of Geophysics and Geomatics, China University of Geosciences, Wuhan 430074, China (e-mail: qqr0425@163.com).

Q. H. Liu is with the Department of Electrical and Computer Engineering, Duke University, Durham, NC 27708 USA (e-mail: qhliu@duke.edu).

Digital Object Identifier 10.1109/JSTARS.2017.2685628

existing hybrid methods, the combination of wavelet and curvelet transforms is quite universal, robust, and popular in denoising algorithms introduced in recent years [1], [45]–[47]. However, the existing combination of wavelet and curvelet decomposition has improved performance if an optimal threshold can be obtained.

In this paper, the main contribution is that we propose a new denoising strategy based on the HOCS method in the wavelet domain, comprising a 2-D hybrid filter that includes some useful properties of curvelet transforms. It utilizes an optimal sparse representation of seismic data with second-order continuously differentiable singularities in the curvelet domain, and uses the HOCS method to estimate the threshold for the curvelet coefficients. Thus, this hybrid scheme introduces a self-adaptive thresholding technique suitable for field data processing.

The effectiveness of the proposed hybrid scheme is demonstrated two-fold. First, we compare different types of denoising on common-offset seismic profiling contaminated with different types of noise (i.e., Gaussian random and coherent), then discuss the performance of existing techniques compared with the hybrid scheme. For this purpose, the k-wave toolbox (available at www.k-wave.org/forum) is used to implement common-offset seismic profiling in the time domain [48]. Second, all the denoising methods are tested on three common-offset seismic profiles acquired from karst cavity and hidden sinkhole detection studies.

II. Denoising Techniques Applied to Seismic Data

A. Curvelet Transform

In this paper, we apply the second-generation discrete curvelet transform [27], [28]. For this purpose, it is necessary to first apply the 2-D fast Fourier transform [27] to seismic data. Assume that x is the spatial domain variable, ω is the frequency domain variable, and the polar coordinates relate to r and θ in the frequency domain. We construct a pair of window functions for the scale and angle, which are expressed as the radial window $W(r)$ and angular window $V(t)$, respectively, subject to the constraints

$$\sum_{-\infty}^{\infty} W^2(2^j r) = 1 \quad r \in (3/4, 3/2) \tag{1}$$

$$\sum_{-\infty}^{\infty} V^2(t-m) = 1 \quad t \in (-1/2,\ 1/2) \tag{2}$$

where W is defined and supported on $\{1/2, 2\}$ and V is limited to $\{-1, 1\}$ to ensure the smooths are non-negative and real-valued; here, m is the orientation and j is the scale [27]. The windows W in the frequency domain and V are partitioned into annuli $|x| \in \{2^j, 2^{j+1}\}$ and polar wedges $\theta_{j,m} = 2\pi m \cdot 2^{-[j/2]}$, respectively. For each $j \geq 0$, the frequency domain window is given by

$$U_j(r,\theta) = 2^{-3/4} W(2^{-j} r) V(2[j/2] \cdot \theta / 2\pi) \tag{3}$$

where $\{j/2\}$ denotes the integer value. Equation (3) wraps the aforementioned windows about the origin and is defined only by the wavelet scale j and angle θ. For the other scales, the window functions in the frequency domain are denoted $\varphi_j(\omega)$; $\varphi_j(x)$ in the spatial domain is obtained by rotation with angle $\theta_{j,m}$, anisotropic dilation, and translation, with $k = (k_1, k_2)$.

For scale j, orientation $\theta_{j,m}$, and $x_k^{j,m} = R_{j,m}^{-1}(k_1 \cdot 2^{-j}, k_2 \cdot 2^{-j/2})$, the curvelet coefficients can be expressed as

$$\varphi_{j,m,k}(x) = \varphi_j \left[R_{j,m}(x - x_k^{j,m}) \right] \tag{4}$$

where the rotation matrix with respect to angle $\theta_{j,m}$ is given by

$$R_{j,m} = \begin{pmatrix} \cos\theta & \sin\theta \\ -\sin\theta & \cos\theta \end{pmatrix}. \tag{5}$$

Finally, for $f(x) \in L^2(R^2)$ the curvelet transform is given by

$$C(j,m,k) = \langle f, \varphi_{j,m,k} \rangle = \int_{R^2} f(x) \overline{\varphi_{j,m,k}(x)} dx. \tag{6}$$

An inverse Fourier transform on a special sheared grid is used to transform the frequency-domain data to the spatial domain. To overcome the poor performance of the conventional FFT on a nonuniform grid, a uniquely spaced FFT or wrapping technique [28] is used in the second-generation discrete curvelet transform.

B. Wavelet-Based HOCS Method

Multiresolution wavelet analysis is implemented in the transform domain by mapping a discrete signal onto an approximation space and a detail space [16], [49]. With the two spaces covered by discrete-time sub-band decomposition, the input signal is then filtered into a lowpass (approximation) and highpass (detail) window, which are also called the scaling and wavelet functions, respectively. For piecewise smooth 1-D wavelets, when isolating discontinuities with point-like characteristics in two dimensions, thresholding the curvelet coefficients has been proposed for seismic data denoising. HOCS in the wavelet domain is one such thresholding scheme, in which the threshold value is obtained using higher order statistics.

In this paper, we apply the HOCS using 1-D and 2-D wavelets. This algorithm is implemented in four steps:

1) applying a 1-D or 2-D discrete wavelet transform to the data;
2) obtaining the correlation coefficients of the data set from higher order statistics;
3) stacking the aforementioned data after incorporating the correlative coefficients; and
4) applying a 1-D or 2-D inverse wavelet transform.

For scale and translation indices j and k, a time series $f(t)$ can be written in terms of its wavelet coefficients as

$$f(t) = \sum_{j=-\infty}^{+\infty} \sum_{k=-\infty}^{+\infty} d_{j,k} \tilde{\psi}_{j,k}(t) \tag{7}$$

where the relevant decomposition coefficients are

$$d_{j,k} = \left\langle f(t), \tilde{\psi}_{j,k}(t) \right\rangle \tag{8}$$

and $\tilde{\psi}_{j,k}(t)$ is the wavelet basis. In this work, we use a length 16 symmlet (i.e., least asymmetric wavelet) that has eight vanishing moments.

The key idea of using correlation coefficients obtained from higher order statistics for seismic denoising is that the higher order statistical spectrum of a Gaussian signal is zero. Suppose that a pair of time series $f_i(t)$ and $f_{i+1}(t)$ represent seismic records gathered simultaneously by adjacent sensors. Let $i = 1, 2, ..., M$ denote the sensor number and $t = 1, 2, ..., N$ the times of discrete samples. Let $F_i^k(m)$ denote the 1-D or 2-D wavelet transform of $f_i(t)$ at scale k and translation window length $2P + 1$; P= 1 if three adjacent data sets are used for correlation. The third-order correlation function without migration [16], [49] is defined by

$$r_{i,i+1,i}^k(t) = \sum_{m=t-p}^{t+p} F_i^k(m) F_{i+1}^k(m) F_i^k(m) \tag{9}$$

and the corresponding normalization is

$$\overline{r}_{i,i+1,i}^k(t) = \frac{r_{i,i+1,i}^k(t)}{\sqrt{r_{i,i}^k(t) r_{i+1,i+1}^k(t) r_{i,i}^k(t)}} \tag{10}$$

where $r_{i,i}^k(t)$ and $r_{i+1,i+1}^k(t)$ are the second-order autocorrelations of $f_i(t)$ and $f_{i+1}(t)$ in the wavelet domain, respectively. Then, the weighted seismic record is reconstructed from

$$\overline{F}_i^k(t) = \overline{r}_{i,i+1,i}^k(t) F_i^k(t). \tag{11}$$

Since wavelet analysis is roughly equivalent to bandpass filtering, it is possible to reconstruct the original data using the 1-D or 2-D inverse wavelet transform of (11).

C. Hybrid Denoising Scheme in Multiple Domains

Combined wavelet and curvelet schemes have been applied to denoise images by many authors (e.g., [45], [46]). They have also been used for image approximation [47] and are now used extensively in seismic data processing [1], [2]. As demonstrated in a previous work [1], the hybrid denoising scheme overcomes the shortcomings of either single-system (wavelet or curvelet domain) algorithm and circumvents many of the difficulties of seismic processing. In this work, we introduce a hybrid reconstruction algorithm for seismic denoising that improves the final result. The key idea of the hybrid approach is to incorporate the HOCS method into the curvelet transform decomposition, which we will show leads to significant improvement over using either algorithm individually.

The alternation of wavelet and curvelet basis functions is designed at the finest scale for curvelet transforms, in which the two basis functions are applied mainly to remove energy from unwanted angles caused by unfit wedge-shaped support in the frequency domain. For assigning wavelets to the finest levels in a curvelet transform, a so-called "partition of unity" is obtained [27], [28]. At scale j, the unique sample window that isolates the orientation is constructed to obey (3), using the relationship

$$U_j(k_1, k_2) = W_j(k_1, k_2) V_j(k_1, k_2) \tag{12}$$

where the radial window $W_j(k_1, k_2)$ and angular window $V_j(k_1, k_2)$ isolate angle $\theta_{j,m}$.

The next basis function at the finest scale is the curvelet, which obeys (3) and is described in Section II-A. These finest scale curvelets can also be considered sampled standard windows with periodization in the frequency domain, the latter of which is introduced to prevent the confusion that occurs when taking an approximate modulus. The finest scale curvelet still obeys the relationship [27]

$$\sum_j \sum_\theta |U_j(r, \theta)|^2 = 1. \tag{13}$$

However, because the finest scale wavelet is restricted to the concept of directional basis cells, a natural choice is the implementation of the finest scale curvelet basis function in the curvelet transform for the ultimate results in aliased basis functions by overlapping data periodicity in basis elements. The main challenge of the combined algorithm is that point-like and line-shaped edge features must be preserved for useful seismic events after the curvelet transform, while the above features are retained but disordered for coherent noise. It is possible, therefore, to capture the features of useful signals with good correlations at all scales and all angles, then to remove the features of coherent noise with disordered correlations. The HOCS in the wavelet domain has this property [23], [25].

Given the above, the hybrid denoising scheme proposed in this work is implemented by first applying a curvelet transform, then using the HOCS method to identify the curvelet coefficients of seismic events in the wavelet domain. Thus, the architecture of the hybrid denoising scheme in multiple domains is as follows:

Step 1: Take the curvelet transform of the original signals $f_i(t)$ to the finest scale to obtain curvelet coefficients $C_{j,\theta}$ for all possible scales and angles.

Step 2: For $j = 1, 2, \ldots, J$ do

For $\theta = 1, 2, \ldots, \vartheta$ do

For all sensors

For $i = 1, 2, \ldots, M - 1$ do

Take the wavelet transform of $C_{j,\theta}(i)$, $C_{j,\theta}(i + 1)$ to obtain Wt_i, Wt_{i+1}.

Retain the approximation coefficient W_{af} and detail coefficient W_{df} for all scales in the wavelet domain.

For $j_c = 1, 2, \cdots, J_C$ do

Calculate the correlation coefficient r_c of $W_{\mathrm{af}}(i, j_c)$ and $W_{\mathrm{af}}(i + 1, j_c)$ using higher order statistics.

Let $W_{\mathrm{df}} = 0$.

Compute the weighted data stack, $\tilde{W}t_i = Wt_i(W_{\mathrm{af}}, W_{\mathrm{df}}) \cdot r_c$

Take the inverse wavelet transform of $\tilde{W}t_i$ to obtain the denoised curvelet coefficients $f_{\mathrm{wt}}(i)$.

Step 3: Take the inverse curvelet transform of each f_{wt} to yield the denoised data, f_{cwt}.

In the architecture of the hybrid denoising scheme, the number of scales is $J = 3$ and the number of angles at the second coarsest level is $\vartheta = 16$ as default set in curvelet code [27], [28]. For HOCS in wavelet code, the number of scales is $J_C = 3$ and the wavelet basis is "sym8," which is the same

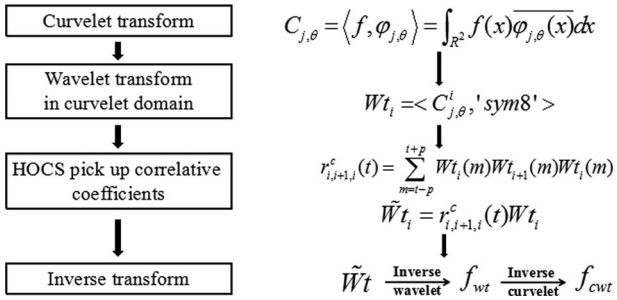

Fig. 1. Flow chart of the hybrid denoising scheme.

as chosen in previous seismic or electromagnetic studies [23], [25].

For the above-mentioned denoising steps, there is no need to use an ad hoc rule to determine a hard threshold for synthetic or measured data sets; indeed, such thresholding values are provided by the HOCS method, as shown in Fig. 1.

III. Numerical Validation

The accuracy and efficiency of the proposed hybrid multidomain denoising scheme for seismic data interpretation are now demonstrated by extracting useful signals from contaminated data and comparing the proposed scheme with other denoising methods. Raw seismic data are usually contaminated by noise in practical applications, such as the noise caused by the presence of near-surface inhomogeneities, inconsistent sensors, and intrinsic noise in equipment. Here, we design synthetic seismic data contaminated with zero-mean Gaussian noise and coherent noise. To evaluate the performance of the method introduced in this paper, we use the peak signal-to-noise ratio (PSNR)

$$\mathrm{PSNR} = 20\log_{10}\left(\frac{\max\{S\}}{\sqrt{\frac{1}{NM}\sum_{n=1}^{N}\sum_{m=1}^{M}\left|S_{n,m}-\tilde{S}_{n,m}\right|^2}}\right) \tag{14}$$

where S and $\tilde{S}$ are the original and denoised seismic data, respectively. The PSNR is calculated using a peak value of S and a mean squared error between S and $\tilde{S}$. Thus, a higher PSNR indicates that more energy is recovered from the contaminated data. If the residual noise remains dominant, then the refocused energy will be worse, and will cause a significantly lower PSNR. In the following case studies, the decibel (dB), the standard unit for PSNR, is used. The color scales of all corresponding 2-D figures denote the amplitudes of seismic data.

A. Comparisons of Curvelet Transforms

To obtain synthetic seismic data, a 2-D cavity object embedded in a multilayered background medium with layer interfaces parallel to the x axis is shown in Fig. 2. Each layer is characterized by a unique velocity and density. The seismic profiling is obtained with one monopole source (Tx) and one sensor (Rx) rolling movement with a common offset. In this work, the synthetic data are simulated by the k-wave tool, in which full wave simulations in the forward solution are obtained by the

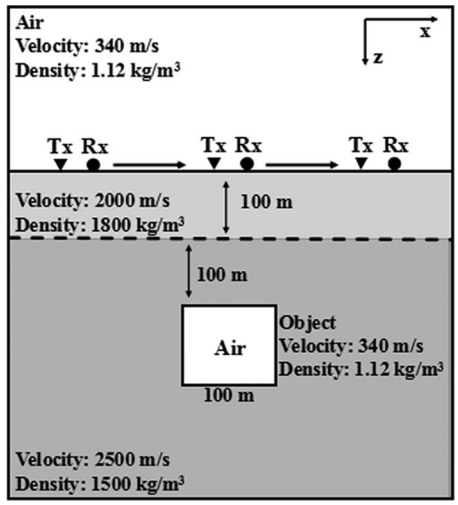

Fig. 2. Geometry of a 2-D cavity object embedded in a multilayered medium for a common-offset seismic profile.

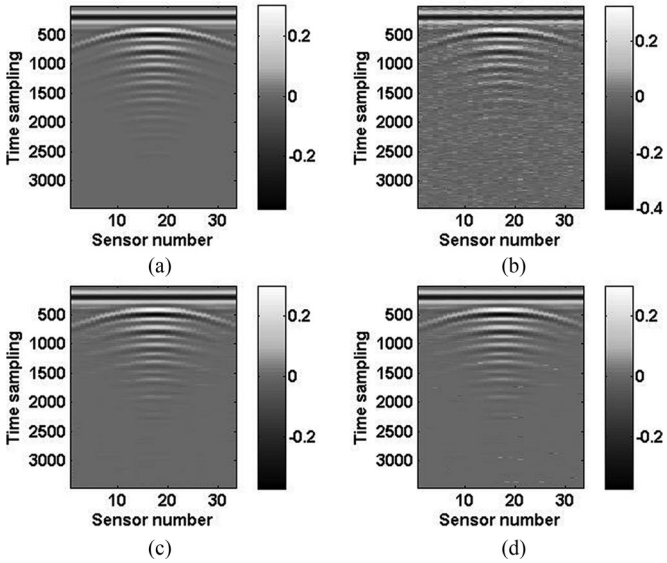

Fig. 3. Denoising results using curvelets with a correct hard thresholding value. (a) Original data. (b) Data contaminated by Gaussian white noise. (c) Denoising by curvelet basis. (d) Denoising by wavelet basis.

pseudospectral time-domain method [50]. For details, the reader can refer to [48]. For time-domain modeling, the time function of the monopole source is chosen to be the first derivative of a Blackman–Harris window function.

The test case is designed to validate the reconstruction for continuous and multiple curve-like seismic events caused by the interface of layered media and a rectangular cavity, as shown in Fig. 3(a). The fast discrete curvelet transform used here was introduced in [28] and is available at www.curvelet.org.

Denoising results for the curvelet transform with a curvelet (20.51 dB) and wavelet basis (19.97 dB) representation of seismic data (8.5 dB) contaminated by Gaussian noise are presented in Fig. 3(b)–(d). It is clear that the reconstructed results are refocused back to original energy with a higher PSNR than the noisy data with an appropriate hard thresholding value δ. Such a correct thresholding value is chosen as the percentage of noisy

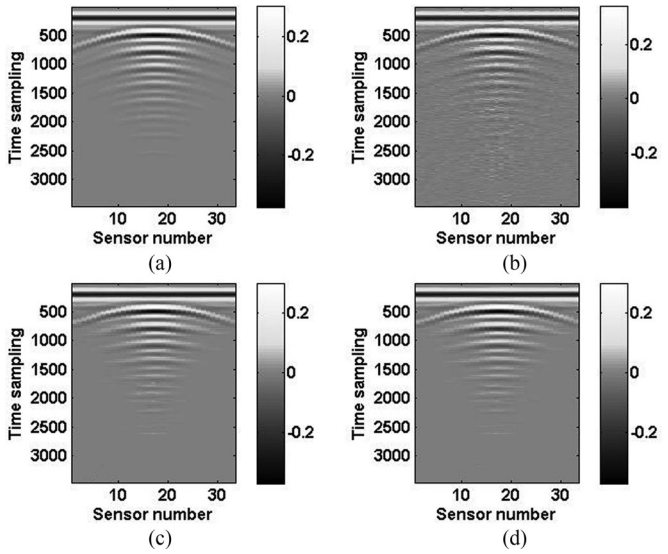

Fig. 4. Denoising results using curvelets with a correct hard thresholding value. (a) Original data. (b) Data plus coherent Gaussian noise. (c) Denoising by curvelet basis. (d) Denoising by wavelet basis.

TABLE I
PSNRS OF DENOISING RESULTS BY CURVELETS WITH A CURVELET AND WAVELET BASIS FOR DIFFERENT HARD THRESHOLDING VALUES (δ, WHICH IS THE PERCENTAGE OF NOISY AND ORIGINAL DATA)

δ(%)		Curvelet basis (dB)	Wavelet basis(dB)		Curvelet basis(dB)	Wavelet basis(dB)
15	White	17.44	15.87	Coherent	11.52	11.54
20	Gaussian noise	20.38	18.88	Gaussian noise	11.47	11.46
25	(PSNR = 11.36)	22.41	21.84	(PSNR = 11.38)	11.54	11.52
35		22.11	22.15		11.39	11.43
60		19.12	19.32		12.49	13.85
100		15.42	15.24		18.36	18.38
130		13.75	13.56		16.45	16.55
180		12.52	11.38		13.50	13.45

and original data. Now, let us turn to more realistic applications of denoising. To do this, synthetic data are contaminated with coherent Gaussian noise, in which the amplitude of the noise is proportional to the amplitude of the original data. In the first case, the Gaussian noise floor does not change with that of the signal; i.e., whether a signal exists or not, the noise will always be there. For coherent Gaussian noise, the sensor in the array that has the strongest signal has the desired SNR, but all other sensors should have poorer SNR values. The signals are also contaminated with random noise (11.38 dB), as shown in Fig. 4(b). Denoising results obtained using a curvelet transform with a curvelet (18.37 dB) and wavelet basis (18.46 dB) are presented in Fig. 4(c) and (d). Again, the reconstructed results are denoised well, with a correct hard thresholding value.

Table I lists the PSNR values obtained by denoising with curvelets with a curvelet and wavelet basis at different hard thresholding values. From the presented numerical denoising results, it is necessary for the analyst to supply a reasonable hard thresholding value to yield a well-reconstructed result when implementing the available curvelets algorithm (at www.curvelet.org). The difference in PSNR is about 7 dB between the highest and lowest values, regardless of whether or not the noise is coherent. Thus, the choice of an appropriate threshold is fundamental to curvelet denoising. Although abundant methods from different fields have been proposed for choosing optimal threshold values (e.g., [1], [51]), a thorough review of the topic lies beyond the scope of this paper. PSNRs for denoising with a curvelet basis are generally higher than those obtained using a wavelet basis alone; we, therefore, use a curvelet basis for the curvelet transform in the following case studies.

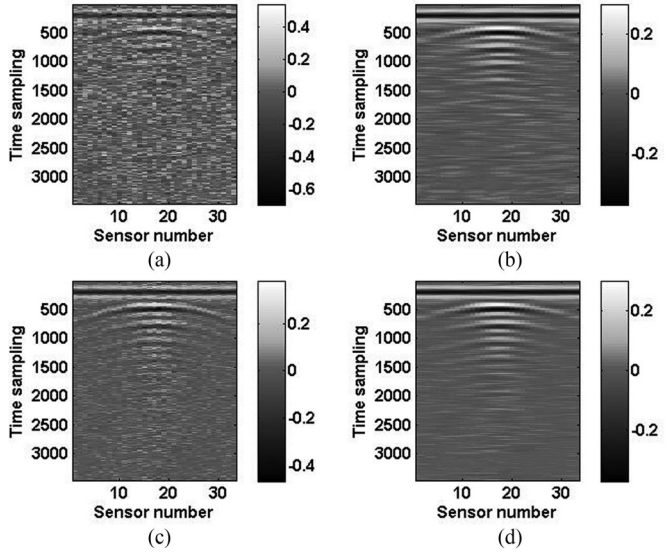

Fig. 5. Denoising results using curvelets with an approximate hard thresholding value for increasingly noisy data (as compared with those in Figs. 3 and 4). (a) Data contaminated by additive Gaussian noise. (b) Denoised data from (a). (c) Data contaminated by coherent additive Gaussian noise. (d) Denoised data from (c).

As shown in Fig. 5(a) and (c), curvelet denoising alone, in which approximate hard thresholding is used, is increasingly ill-suited to noisy data as the noise levels increase (as compared with those in Figs. 3 and 4). There are many ways to compute the approximate hard thresholding, e.g., by computing the norm of each individual curvelet. The residual noisy segments after curvelet denoising has been applied are disorderly and unsystematic when the noise level increases, whereas the features of seismic events are preserved with a high degree of consistency [see Fig. 5(b), 6.86 dB]. The coherent parts of the noisy data are presented as continuous events, as the useful signals from the seismic target in Fig. 5(d) with the PSNR of 8.73 dB. Without an appropriate hard threshold, in field data interpretation, such false features always cause a waste of money for exploration validation, due to inaccurate drilling locations.

B. Comparisons of HOCS in the Wavelet Domain

We now compare HOCS with the individual denoising method (curvelet basis) at the same noise levels (see Fig. 5) using the method of PSNR measurements of contaminated random and coherent noise. This HOCS algorithm is implemented in the wavelet domain. In this work, 1-D and 2-D wavelet transforms are chosen for all of the above-mentioned cases.

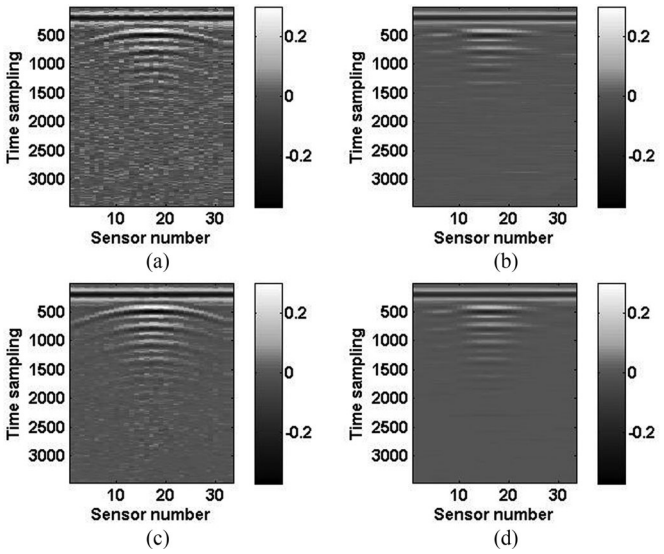

Fig. 6. Denoising results using the HOCS method. (a) and (b) The results of denoising the data in Fig. 5(a) using 1-D and 2-D wavelets, respectively; and (c) and (d) the corresponding results for the data in Fig. 5(c).

As discussed above, the correlative statistics is worked in a single direction; i.e., in the time domain. Therefore, any denoising improvement is restricted to the correlative direction when the original data are transformed with a 1-D wavelet. This phenomenon is shown in Fig. 6(a) and (c) for increasingly noisy data. Fig. 6(a) shows the reconstructed result for Gaussian white noise (3.5 dB), where the shape, location, and signal amplitude of the original data are basically recovered for the continuous and multiple curve-like events. The reconstructed result for a signal with coherent additive noise (2.79 dB) is presented in Fig. 6(c), in which most of the coherent noise events are identified and removed with a PSNR of 11.33 dB. From the above-mentioned results, it is obvious that the reconstructive abilities of the 1-D HOCS are quite different to the results shown in Fig. 5. In particular, for data with additive white noise, it is difficult to obtain a clear result with 1-D HOCS, but the PSNR of 1-D HOCS is higher than for curvelets. Thus, it is possible to combine the HOCS and curvelets to improve the reconstructed results.

We now demonstrate the use of a 2-D HOCS to improve the above-mentioned denoising results. The key difference between this and the 1-D algorithm is that the wavelet transform is 2D, whereas the correlative statistic only works in the time domain. With such a denoising scheme, the 2-D HOCS is expected to provide clear images for the random and coherent noisy data in the horizontal, vertical, and diagonal directions, as presented in Fig. 6(b) and (d) with the PSNRs of 5.57 and 5.8 dB. The reconstructed results are "smoothed" similar to the original data, especially for the continuous seismic events; the shape, location, and signal amplitude of the original data are reconstructed well. However, the curve-like seismic events are discontinuous with a "step-like" visual appearance, which may be caused by computing the correlative statistic in only 1D. In the following case studies, we choose the 1-D HOCS method for comparisons of seismic data denoising.

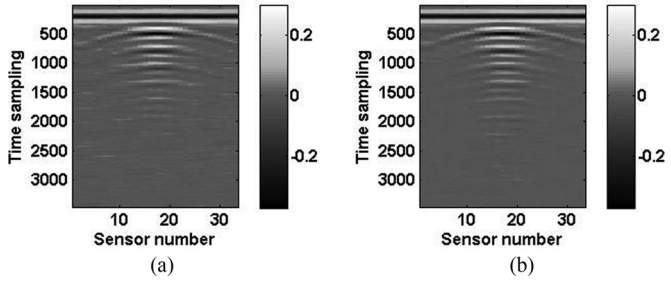

Fig. 7. Denoising results with a hybrid denoising scheme. (a) Denoising results for the data in Fig. 5(a), a signal with additive Gaussian white noise. (b) Denoising results for the data in Fig. 5(c), a signal with coherent Gaussian noise.

C. Comparison of the Hybrid Denoising Scheme

In this section, we test the effectiveness of the hybrid denoising scheme in reconstructing the original data with fixed noise levels, as shown in Fig. 5(a) for Gaussian white noise and Fig. 5(c) for coherent Gaussian noise. All parameters used in the individual curvelets in Section III-A, including those used in 1-D HOCS in Section III-B, are adopted and kept unchanged in this hybrid denoising scheme.

As the curvelet transform first works with the curvelet basis function at the finest scale in our hybrid denoising scheme, it is expected to transform the useful seismic events and noise to different scales and different angles in the curvelet domain. The correlative statistic is designed to detect and increase the coefficients of useful seismic events in the reconstructed transform, because the correlation between residual point-like and line-edge-like noises is weaker than in dominating events. The main advantage of this hybrid denoising scheme is that hard thresholding values are not required for the curvelet transform.

Comparing the reconstructed results of Figs. 7 with 3(a), it is clear that the shapes, locations, and signal amplitudes of continuous and curve-like seismic events are well recovered compared with the original data. One can see the significance of using the hybrid denoising scheme in seismic textures clearly in PSNR numbers via comparison with those provided in the above-mentioned denoising algorithms (see Figs. 5 and 6). Numerical values of the PSNR presented in Table II show that this hybrid algorithm outperforms the alternative algorithms described above; a maximum value of 10 dB is achieved with Gaussian white noise and 11.72 dB with coherent Gaussian noise, compared with the results shown in Figs. 5 and 6. The PSNR of the hybrid denoising scheme is about 1–4 dB higher than that of curvelets or HOCS alone. This is because the advantages of the individual systems are combined in this hybrid scheme.

Fig. 8 shows the comparative amplitude-preserving properties of individual denoising algorithms and the hybrid method for data with additive Gaussian white noise, using a sample recorded at sensor location 18 [see Fig. 7(a)]. As the Gaussian white noise increases, the original data become completely masked by noise, and it is difficult to manually identify useful seismic events, as shown in Fig. 8. Reconstructed signals using individual denoising systems and the hybrid denoising scheme are exhibited and compared with the original data (black line).

TABLE II
PSNRS OF DENOISING RESULTS BY DIFFERENT DENOISING SCHEMES

Denoising scheme		Correct δ (%)	White Gaussian noise (PSNR = 8.5 dB)	Coherent Gaussian noise (PSNR = 11.38 dB)	Approximate δ (%)	White Gaussian noise (PSNR = 1.47 dB)	Coherent Gaussian noise (PSNR = 2.79 dB)
Curvelet	Curvelet basis	25 % for white noise,	20.51	18.34	46 % for both noises	6.86	8.73
	Wavelet basis	100% for coherent noise	19.97	18.46		–	–
HOCS	1D					3.5	11.33
	2D	–	–	–	–	5.57	5.8
Hybrid scheme						10	12.72

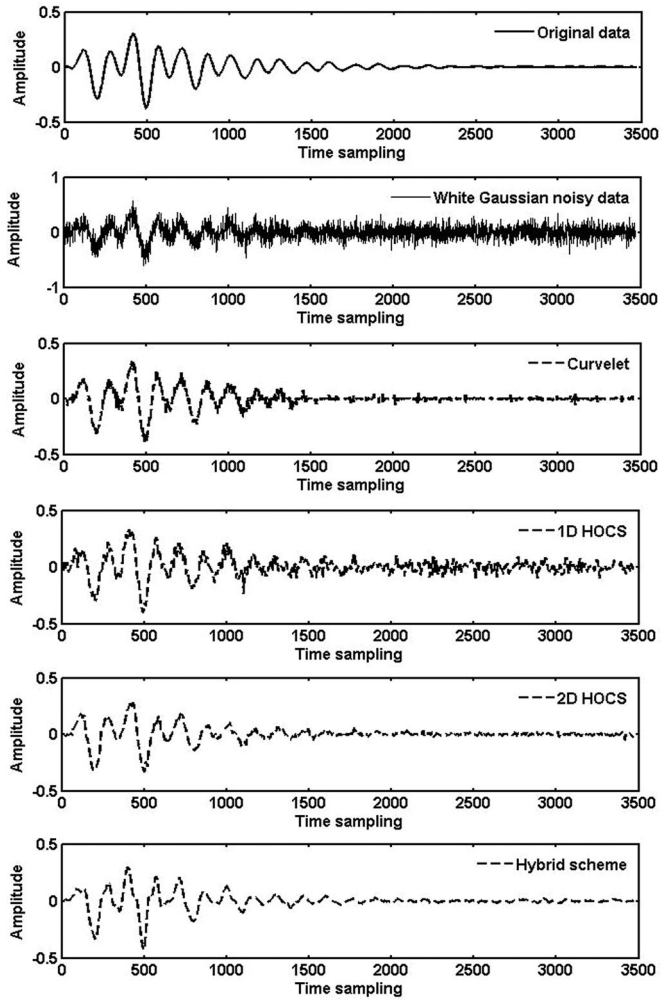

Fig. 8. Denoising results using the individual and hybrid denoising schemes at the 18th sensor location of Fig. 7(a).

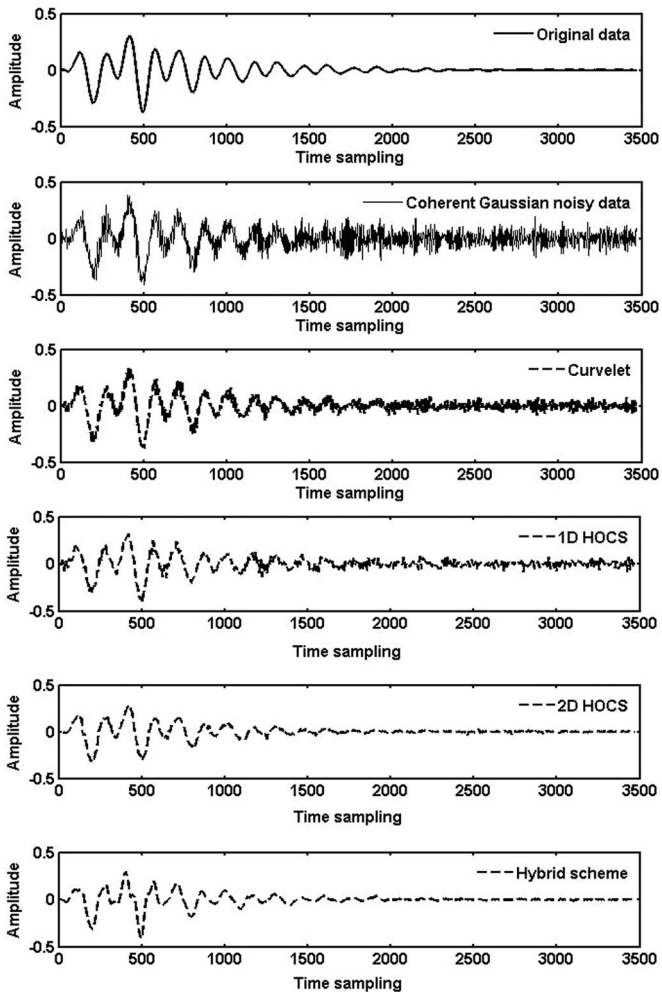

Fig. 9. Denoising results by the individual and the hybrid denoising scheme at the 18th sensor location for Fig. 7(b).

All of the methods preserve the basic amplitude values of the dominant seismic events, but the hybrid method shows great improvement over the other methods in terms of amplitude values and the smoothness of the denoising data.

Fig. 9 illustrates the relative amplitude-preserving abilities of the individual denoising algorithms and the hybrid method with data contaminated by coherent Gaussian noise from Fig. 7(b), taken at sensor location 18. The noisy data are not visibly improved using curvelets with a curvelet basis at the finest scale. The reconstructed results from the 1-D and 2-D HOCS method are better than the former results with coherent additive Gaussian noise because the denoising process takes advantage

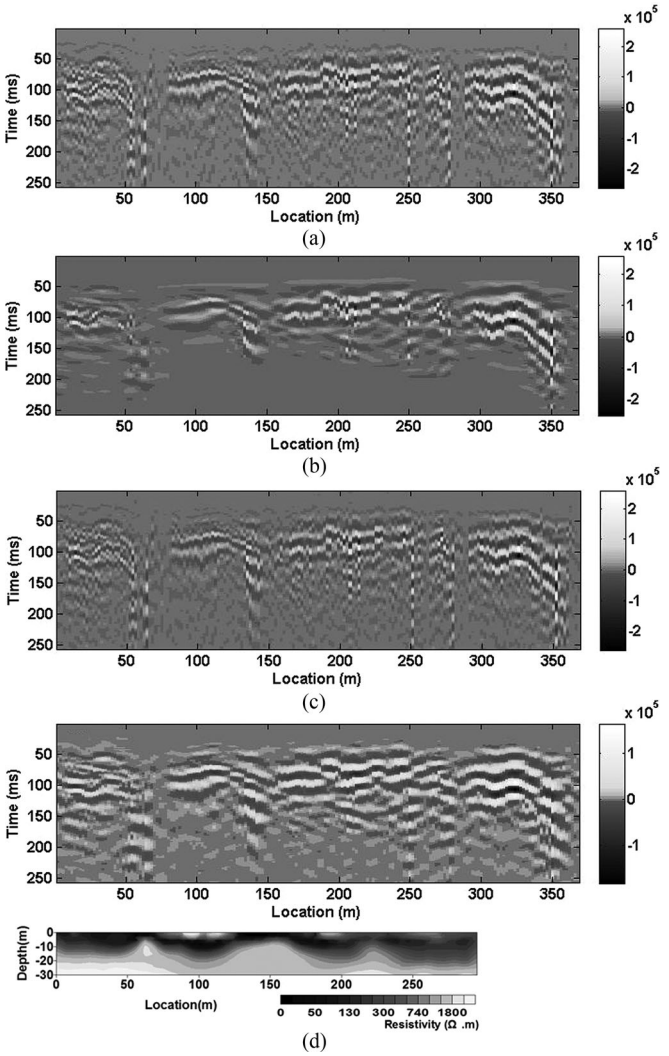

Fig. 10. Denoising results compared with resistivity imaging. (a) Original field data. (b) Data denoised by a curvelet transform. (c) Data denoised by 1-D HOCS. (d) Data denoised by the hybrid scheme.

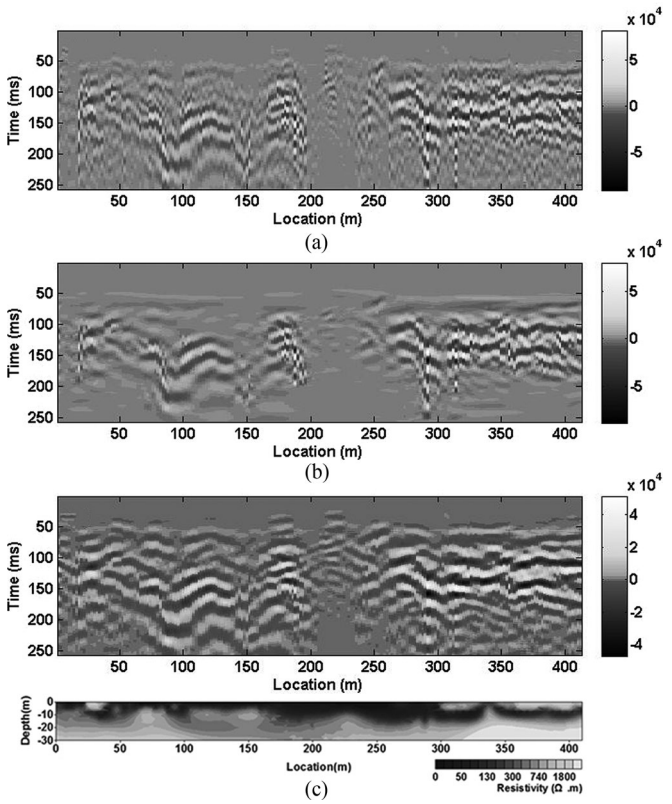

Fig. 11. Denoising results compared with resistivity imaging. (a) Original field data. (b) Data denoised using curvelets. (c) Data denoised using the hybrid scheme of this study.

of the correlative statistic. The hybrid denoising scheme thus provides a higher quality result than all other results, by preserving both continuous and curve-shaped features of seismic waveforms.

IV. Field Data Analysis

We now test the effectiveness of the hybrid denoising scheme on three common-offset seismic profiles acquired from karst cavity and hidden sinkhole detection studies after artificial backfill. In seismic surveys conducted for these purposes, seismic records are generally contaminated with three kinds of noise:

1) random noise caused by measurement systems or inherent uncertainties;
2) diffracted waves that arise from the boundaries of the hidden cavity or sinkhole; and
3) "jumping" seismic events formed by shallow heterogeneities in local structure.

The random noise does not change with the target signal; whether a useful signal exists or not, the noise is always present. Diffracted waves are incorporated into seismic events as discontinuous or curve-like features. Local heterogeneities introduced during or after artificial backfill lead to damaged or missing seismic data. The challenge of such a seismic survey, then, is clearly monitoring karst cavities and hidden sinkholes with high resolution and fidelity.

A. Single Cavity Detection

The first seismic survey is designed and presented in Fig. 10(a), in which the seismic records are contaminated with the three types of noise described above. In this case, the task of denoising is recovering the continuity of the jumping seismic events. Fig. 10(b)–(d) shows the results of denoising by individual systems and the hybrid scheme proposed in this paper. In Fig. 10(b), the result is denoised using curvelets with an approximate hard threshold determined from the L2 norm of field data. Most of the dominant seismic events are barely retained, and the random noise is mostly removed. However, the damaged and discontinuous features presented in Fig. 10(b) are aggravated by using curvelets with approximate hard thresholding. It is also obvious that the continuity of the jumping seismic events cannot be reconstructed with curvelets alone.

The denoising results in Fig. 10(c) use a 1-D HOCS method, and are close to the original seismic data in Fig. 10(a). As the

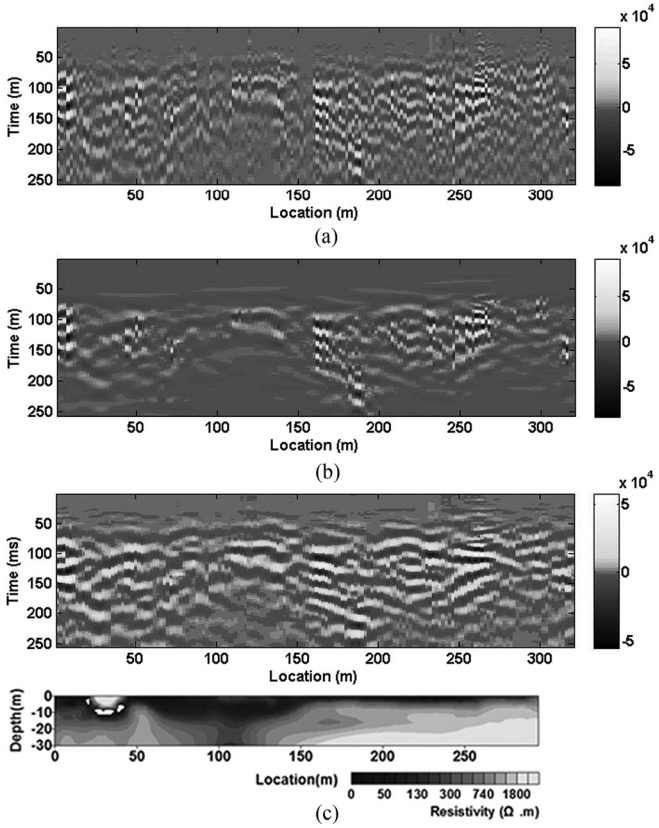

Fig. 12. Denoising results compared with resistivity imaging. (a) Original field data. (b) Data denoised using curvelets. (c) Data denoised using the hybrid scheme of this work.

1-D wavelet transform is applied to adjacent sensors in the HOCS method, the coefficients in the transform domain are enlarged for continuous seismic events. However, the damaged and jumping seismic events are aggravated by the 1-D HOCS method. Slight changes in the removal of random noise are also present. Thus, jumping seismic events are isolated in the denoising results by the 1-D HOCS method, which is not considered in the subsequent field data analysis.

Denoising with a hybrid scheme is exhibited in Fig. 10(d). In the hybrid process, the field data are transformed by curvelets using multiple scales and multiple angles, in which the useful seismic and noisy components are separated into different angles. The 1-D HOCS method is then applied to identify and preserve the damaged seismic information in the curvelet domain. It is also clear from the denoising result that the random noise is well whitened, while the jumping coherent noise is recovered and the damaged seismic events are well preserved with good correlations. Thus, the hybrid scheme shows great improvements over other methods, not only with respect to denoising, but with respect to preserving useful seismic information.

To evaluate the performance of the hybrid scheme in field data analysis, denoising results using individual systems and the hybrid scheme are compared with resistivity imaging in Fig. 10. From the results obtained by individual systems (curvelets and 1-D HOCS), one can identify three regions (50–100, 150–200, and 250–300 m) caused by hidden cavity-like seismic features. As shown by the hybrid denoising result and resistivity imaging, the location of the hidden cavity is most likely in the range 50–100 m.

B. Double Cavity Detection

A second seismic survey, conducted to detect multiple cavities embedded in artificial backfill, is presented in Fig. 11(a). We observe two cavity-like seismic events found at 50–200 m, and a wide range of damaged and absent seismic events at 200–300 m. The problems in this survey are that the curve-like seismic events that arise from the double cavities are complicated and distorted by random noise, and damaged seismic events compound the difficulty of accurate interpretation. In Fig. 11(b), denoising with curvelets mainly preserves the curve-like features of useful seismic events while removing much of the noise, but the seismic events are discontinuous and the damaged region (200–300 m) cannot be recovered. Fig. 11(c) shows denoising result with a hybrid scheme, which provides clear, continuous seismic events for the double cavities. Most importantly, the damaged seismic events are well-resolved in the 200–300 m region, in which convex seismic events appear at early propagation times and vanish at later times. It is possible that the moister backfill is located at shallow depths and leads to greater attenuation of seismic power. The above-mentioned phenomena suggested by hybrid denoising are corroborated by the resistivity imaging in Fig. 11, notably in the locations of the double cavities (50–200 m) and low resistivity values consistent with moist backfill (200–300 m).

C. Hidden Sinkhole Detection

In this section, denoising is applied to a case study consisting of a seismic survey for hidden sinkhole detection. As shown in Fig. 12(a), the seismic records are contaminated by so-called "salt and pepper noise" and isolated jumping seismic waves can be seen. It is difficult to determine the most plausible location of the hidden sinkhole. Fig. 12(b) and (c) presents denoising results using curvelets and the hybrid scheme, respectively. In Fig. 12(b), the curvelets whiten the salt and pepper noise but degrade the seismic information at later propagation times. The hybrid scheme used in Fig. 11(c) outperforms curvelets alone by removing the noise and better clarifying the location of the hidden sinkhole (50–150 m), as corroborated by the resistivity imaging.

V. Conclusion

To whiten random noise and identify coherent noise for preserving prominent seismic features, a hybrid denoising scheme is proposed. The main idea of the method is to use wavelet-based HOCS in an algorithm to reconstruct seismic events in the curvelet domain. This method fully utilizes the optimal sparse representation of objects in curvelets and incorporates the HOCS method concept into the denoising procedure. The feasibility and effectiveness of the method are demonstrated through numerical simulations and detections using real seismic records.

Comparisons with denoising algorithms that use only one of curvelets or HOCS show that the hybrid scheme outperforms both. Numerical simulations show that the hybrid scheme significantly improves the ability to remove noise and to recover the continuity of damaged seismic events without the necessity to approximate a threshold. The robustness of the hybrid denoising scheme at different PSNRs has also been investigated. Comparative testing of our technique and single-transform denoising methods on field seismic data shows that our hybrid scheme has the advantage of reconstructing useful seismic events without sacrificing fidelity.

ACKNOWLEDGMENT

The authors would like to thank the Reviewers and the Editor (Prof. A. Plaza) of the IEEE TRANSACTIONS ON GEOSCIENCE AND REMOTE SENSING very much for their helpful comments to improve the quality of our manuscript. The authors would also like to thank the Editor for the review of the manuscript.

REFERENCES

[1] H. Shan, J. Ma, and H. Yang, "Comparisons of wavelets, contourlets and curvelets in seismic denoising," *J. Appl. Geophys.*, vol. 69, no. 2, pp. 103–115, 2009.

[2] J. Ma and G. Plonka, "A review of curvelets and recent applications," *IEEE Signal Process. Mag.*, vol. 27, no. 2, pp. 118–133, Mar. 2010.

[3] X. Han, H. Lin, Y. Li, H. Ma, and X. Zhao, "Adaptive fission particle filter for seismic random noise attenuation," *IEEE Geosci. Remote Sens. Lett.*, vol. 12, no. 9, pp. 1918–1922, Sep. 2015.

[4] Y. Chen and Z. Jin, "Simultaneously removing noise and increasing resolution of seismic data using waveform shaping," *IEEE Geosci. Remote Sens. Lett.*, vol. 13, no. 1, pp. 102–104, Jan. 2016.

[5] A. A. Duchkov, F. Andersson, and M. V. de Hoop, "Discrete almost-symmetric wave packets and multiscale geometrical representation of (seismic) waves," *IEEE Trans. Geosci. Remote Sens.*, vol. 48, no. 9, pp. 3408–3423, Sep. 2010.

[6] G. Tang and J. Ma, "Application of total-variation-based curvelet shrinkage for three-dimensional seismic data denoising," *IEEE Geosci. Remote Sens. Lett.*, vol. 8, no. 1, pp. 103–107, Jan. 2011.

[7] L. T. Duarte, D. Donno, R. R. Lopes, and L. M. T. Romano, "Seismic signal processing: Some recent advances," in *Proc. 2014 IEEE Int. Conf. Acoustics, Speech Signal Process.*, 2014, pp. 2362–2366.

[8] M. Xiong, Y. Li, and N. Wu, "Random-noise attenuation for seismic data by local parallel radial-trace TFPF," *IEEE Trans. Geosci. Remote Sens.*, vol. 52, no. 7, pp. 4025–4031, Jul. 2014.

[9] B. Wang, X. Chen, J. Li, and J. Cao, "An improved weighted projection onto convex sets method for seismic data interpolation and denoising," *IEEE J. Sel. Topics Appl. Earth Observ. Remote Sens.*, vol. 9, no. 1, pp. 228–235, Jan. 2016.

[10] Q. Zhou, J. Gao, Z. Wang, and K. Li, "Adaptive variable time fractional anisotropic diffusion filtering for seismic data noise attenuation," *IEEE Trans. Geosci. Remote Sens.*, vol. 54, no. 4, pp. 1905–1917, Apr. 2016.

[11] Y. J. X, J. X. Cao, D. X. Wang, H. K. Du, and Y. Yao, "Application of the variational-mode decomposition for seismic time–frequency analysis," *IEEE J. Sel. Topics Appl. Earth Observ. Remote Sens.*, vol. 9, no. 8, pp. 3821–3830, Aug. 2016.

[12] S. Warden, S. Garambois, P. Sailhac, L. Jouniaux, and M. Bano, "Curvelet-based seismoelectric data processing," *Geophys. J. Int.*, vol. 190, no. 3, pp. 1533–1550, 2012.

[13] G. Saracco, F. Moreau, P. E. Mathé, D. Hermitte, and J. M. Michel, "Multiscale tomography of buried magnetic structures: Its use in the localization and characterization of archaeological structures," *Geophys. J. Int.*, vol. 171, no. 1, pp. 87–103, 2007.

[14] G. Mauri, G. Williams-Jones, G. Saracco, and J. M. Zurek, "A geochemical and geophysical investigation of the hydrothermal complex of Masaya volcano, Nicaragua," *J. Volcanol. Geotherm. Res.*, vol. 227, pp. 15–31, 2012.

[15] A. Gholami and M. D. Sacchi, "A fast and automatic sparse deconvolution in the presence of outliers," *IEEE Trans. Geosci. Remote Sens.*, vol. 50, no. 10, pp. 4105–4116, Oct. 2012.

[16] S. Gaci, "The use of wavelet-based denoising techniques to enhance the first-arrival picking on seismic traces," *IEEE Trans. Geosci. Remote Sens.*, vol. 52, no. 8, pp. 4558–4563, Aug. 2014.

[17] A. Roueff, J. Chanussot, and J. I. Mars, "Estimation of polarization parameters using time–frequency representations and its application to waves separation," *Signal Process.*, vol. 86, no. 12, pp. 3714–3731, 2006.

[18] Y. Xue, J. Cao, R. Tian, H. Du, and Y. Yao, "Wavelet-based spectrum decomposition of seismic data and its application in hydrocarbon detection," *Geophys. Prospecting*, vol. 64, pp. 1441–1453, 2016.

[19] A. K. Vuong, J. Zhang, R. L. Gibson Jr., and W. W. Sager, "Application of the two-dimensional continuous wavelet transforms to imaging of the Shatsky Rise plateau using marine seismic data," Geological Society of America Special Papers 511, 2015.

[20] S. Ventosa *et al.*, "Adaptive multiple subtraction with wavelet-based complex unary Wiener filters," *Geophysics*, vol. 77, no. 6, pp. V183–V192, 2012.

[21] S. Chopra and K. J. Marfurt, "Choice of mother wavelets in CWT spectral decomposition," in *Proc. SEG Annu. Meeting*, 2015, pp. 1–5.

[22] J. C. Robinson, "Statistically optimal stacking of seismic data," *Geophysics*, vol. 35, no. 3, pp. 436–446, 1970.

[23] S. Z. Zhang and Y. X. Xu, "Higher-order correlation stacking for seismic data in the wavelet domain," *Chin. J. Geophys.*, vol. 49, no. 2, pp. 554–560, 2006.

[24] C. Jiang, Y. Li, N. Wu, G. Zhuang, and H. Ma, "Radial-trace time–frequency peak filtering based on correlation integral," *IEEE Geosci. Remote Sens. Lett.*, vol. 11, no. 9, pp. 1594–1598, Sep. 2014.

[25] J. Li, Z. He, and Q. H. Liu, "Higher-order statistics correlation stacking for dc electrical data in the wavelet domain," *J. Appl. Geophys.*, vol. 99, pp. 51–59, 2013.

[26] H. Zhang, T. Liu, and Y. Zhang, "Denoising of seismic data via multi-scale ridgelet transform," *Earthq. Sci.*, vol. 22, no. 5, pp. 493–498, 2009.

[27] E. J. Candès and D. L. Donoho, "New tight frames of curvelets and optimal representations of objects with piecewise C2 singularities," *Commun. Pure Appl. Math.*, vol. 57, no. 2, pp. 219–266, 2004.

[28] E. J. Candès, L. Demanet, D. L. Donoho, and L. Ying, "Fast discrete curvelet transforms," *Multiscale Model. Simul.*, vol. 5, no. 3, pp. 861–899, 2006.

[29] F. J. Herrmann, D. Wang, G. Hennenfent, and P. P. Moghaddam, "Curvelet-based seismic data processing: A multiscale and nonlinear approach," *Geophysics*, vol. 73, no. 1, pp. A1–A5, 2007.

[30] Z. Zhang, X. Zhang, H. Yu, and X. Pan, "Noise suppression based on a fast discrete curvelet transform," *J. Geophys. Eng.*, vol. 7, no. 1, pp. 105–112, 2010.

[31] J. J. Zheng, X. Y. Yin, G. Z. Zhang, G. H. Wu, and Z. S. Zhang, "The surface wave suppression using the second generation curvelet transform," *Appl. Geophys.*, vol. 7, no. 4, pp. 325–335, 2010.

[32] M. S. Oliveira, M. V. C. Henriques, F. E. A. Leite, G. Corso, and L. S. Lucena, "Seismic denoising using curvelet analysis," *Physica A: Statist. Mech. Appl.*, vol. 391, no. 5, pp. 2106–2110, 2012.

[33] R. Neelamani, A. I. Baumstein, D. G. Gillard, M. T. Hadidi, and W. L. Soroka, "Coherent and random noise attenuation using the curvelet transform," *Leading Edge*, vol. 27, no. 2, pp. 240–248, 2008.

[34] A. Zegadi and K. K. Zegadi, "Coherent and random noise attenuation using the intrinsic time-scale decomposition," in *Proc. SEG Annu. Meeting*, 2009, pp. 3322–3326.

[35] D. Wang, R. Saab, O. Yilmaz, and F. J. Herrmann, "Bayesian wavefield separation by transform-domain sparsity promotion," *Geophysics*, vol. 73, no. 4, pp. A33–A38, 2008.

[36] G. A. Lopez and D. J. Verschuur, "Closed-loop surface-related multiple elimination and its application to simultaneous data reconstruction," *Geophysics*, vol. 80, no. 6, pp. V189–V199, 2015.

[37] V. Oropeza and M. Sacchi, "Simultaneous seismic data denoising and reconstruction via multichannel singular spectrum analysis," *Geophysics*, vol. 76, no. 3, pp. V25–V32, 2011.

[38] N. Kreimer and M. D. Sacchi, "A tensor higher-order singular value decomposition for prestack seismic data noise reduction and interpolation," *Geophysics*, vol. 77, no. 3, pp. V113–V122, 2012.

[39] M. Naghizadeh, "Seismic data interpolation and denoising in the frequency-wavenumber domain," *Geophysics*, vol. 77, no. 2, pp. V71–V80, 2012.

[40] D. Bonar and M. Sacchi, "Denoising seismic data using the nonlocal means algorithm," *Geophysics*, vol. 77, no. 1, pp. A5–A8, 2012.
[41] Y. Chen, S. Fomel, and J. Hu, "Iterative deblending of simultaneous-source seismic data using seislet-domain shaping regularization," *Geophysics*, vol. 79, no. 5, pp. V179–V189, 2014.
[42] Y. Liu, S. Fomel, and C. Liu, "Signal and noise separation in prestack seismic data using velocity-dependent seislet transform," *Geophysics*, vol. 80, no. 6, pp. WD117–WD128, 2015.
[43] G. Plonka and J. Ma, "Curvelet-wavelet regularized split Bregman iteration for compressed sensing," *Int. J. Wavelets, Multiresolution Inf. Process.*, vol. 9, no. 1, pp. 79–110, 2011.
[44] Y. Chen, S. Gan, T. Liu, J. Yuan, Y. Zhang, and Z. Jin, "Random noise attenuation by a selective hybrid approach using f– x empirical mode decomposition," *J. Geophys. Eng.*, vol. 12, no. 1, pp. 12–25, 2015.
[45] B. B. Saevarsson, J. R. Sveinsson, and J. A. Benediktsson, "Combined wavelet and curvelet denoising of SAR images," in *Proc. IEEE Int. Geosci. Remote Sens. Symp.*, vol. 6, 2004, pp. 4235–4238.
[46] J. L. Starck, M. K. Nguyen, and F. Murtagh, "Wavelets and curvelets for image deconvolution: A combined approach," *Signal Process.*, vol. 83, no. 10, pp. 2279–2283, 2003.
[47] G. Plonka, S. Tenorth, and D. Roşca, "A new hybrid method for image approximation using the easy path wavelet transform," *IEEE Trans. Image Process.*, vol. 20, no. 2, pp. 372–381, Feb. 2011.
[48] B. E. Treeby and B. T. Cox, "k-Wave: MATLAB toolbox for the simulation and reconstruction of photoacoustic wave fields," *J. Biomed. Opt.*, vol. 15, no. 2, 2010, Art. no. 021314.
[49] X. D. Zhang, *Time Sequence Analysis-Higher-Order Statistics Method*. Beijing, China: Tsinghua Univ. Press, 1996, ch. 1, pp. 1–20.
[50] Y. Q. Zeng and Q. H. Liu, "A multidomain PSTD method for 3D elastic wave equations," *Bull. Seismol. Soc. Amer.*, vol. 94, no. 3, pp. 1002–1015, 2004.
[51] F. Russo, "An image-enhancement system based on noise estimation," *IEEE Trans. Instrum. Meas.*, vol. 56, no. 4, pp. 1435–1442, Aug. 2007.

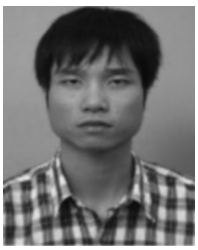

Jing-He Li received the M.S. degree in geodetection and information technology in 2009 from the Guilin University of Technology, Guilin, China, and the Ph.D. degree in geophysics in 2015 from the Institute of Geophysics and Geomatics, China University of Geosciences, Beijing, China.

He is currently a Lecturer with the Guilin University of Technology. His research interests include seismic signal processing, forward and inversion in geophysics.

Yu-Jie Zhang received the M.S. degree in applied mathematics in 2006 and the Ph.D. degree in geodetection and information technology in 2012 from the Institute of Geophysics and Geomatics, China University of Geosciences, Beijing, China.

She is currently a Lecturer with the China University of Geosciences. Her research interests include blind signal processing, time-frequency analysis, and their applications.

Rui Qi received the M.S. degree in computational mathematics from the School of Mathematics and Statistics, Huazhong University of Science and Technology, Wuhan, China, in 2009. He is currently working toward the Ph.D. degree in geodetection and information technology in the Institute of Geophysics and Geomatics, China University of Geosciences, Beijing, China.

His research interests include blind source separation, sparse representation, and compressed sensing.

Qing Huo Liu (S'88–M'89–SM'94–F'05) received the Ph.D. degree in electrical engineering from the University of Illinois at Urbana-Champaign, Champaign, IL, USA, in 1989.

He was a Research Assistant (September 1986 to December 1988) and then a Postdoctoral Research Associate (January 1989 to February 1990) in the Electromagnetics Laboratory, University of Illinois at Urbana-Champaign. From 1990 to 1995, he was a Research Scientist and then a Program Leader with Schlumberger-Doll Research, Ridgefield, CT. From 1996 to 1999, he was an Associate Professor in the Klipsch School of Electrical and Computer Engineering, New Mexico State University, Las Cruces, NM, USA, where he is currently an Adjunct Faculty. Since June 1999, he has been in the Department of Electrical and Computer Engineering, Duke University, Durham, NC, USA, where he is currently a Full Professor. His research interests include computational electromagnetics and acoustics, subsurface sensing, inverse problems, biomedical imaging, simulation of photonic, and high-speed electronic circuits and devices.